Physica E: Low-dimensional Systems and Nanostructures 99 (2018) 75–81

Contents lists available at ScienceDirect

Physica E: Low-dimensional Systems and Nanostructures

journal homepage: www.elsevier.com/locate/physe

Structure, Raman, dielectric behavior and electrical conduction mechanism of strontium titanate

H. Trabelsi [a,*], M. Bejar [a], E. Dhahri [a], M.P.F. Graça [b], M.A. Valente [b], K. Khirouni [c]

[a] Laboratoire de Physique Appliquée, Faculté des Sciences, B.P. 1171, 3000 Sfax, Université de Sfax, Tunisia
[b] I3N and Physics Department, University of Aveiro, 3810-193 Aveiro, Portugal
[c] Laboratoire de Physique des Matériaux et des Nanomatériaux Appliquée à L'environnement, Faculté des Sciences de Gabes Cité Erriadh, 6079 Gabes, Tunisia

ARTICLE INFO

Keywords:
$SrTiO_3$
Raman
Dielectric properties
Relaxation
ac conductivity

ABSTRACT

Strontium titanate was prepared by solid-state reaction method. According to the XRD, it was single phase and has a cubic perovskite structure. The Raman spectroscopic investigation was carried out at room-temperature, and the second-order Raman modes were observed. By employing impedance spectroscopy, the dielectric relaxation and electrical properties were investigated over the temperature range of 500–700 K at various frequencies. The activation energies evaluated from dielectric and modulus studies are in good agreement and these values are attributed to the bulk relaxation. The impedance data were well fitted to an $(R_1//C_1)$-$(R_2//CPE_1)$ equivalent electrical circuit. It could be concluded that the grain boundaries are more resistive and capacitive than the grains. The *ac* conductivity was found to follow the Jonscher's universal dynamic law ω^S and the correlated barrier hopping model (CBH) has been proposed to describe the conduction mechanism.

1. Introduction

$SrTiO_3$ (STO) is an easily functionalizable material that has been the study area of a variety of phenomena [1,2]. It is a wide band-gap, diamagnetic and quantum paraelectric insulator that is used as a suitable substrate for depositing thin films of various oxides such as high-*Tc* superconducting materials [3,4]. At room temperature, the STO adopts cubic perovskite structure possessing close packing of Sr^{2+} with Ti^{4+} occupying the quarter of the octahedral interstices. Below 105 K, it undergoes a structural transition to a tetragonal phase. The dielectric constant follows a Curie–Weiss type law with a Curie–Weiss temperature of ~37 K, as temperature decreases from 300 to 50 K, which indicates a possible paraelectric-ferroelectric phase transition at 37 K [5].

STO ceramic is widely used in microelectronic devices (multilayer capacitors, dynamic random access memory, thermistors, piezo actuators, varistors, etc) by its dielectric properties and thermodynamical stability at high temperature. It exhibits mixed ionic-electronic conduction [6] and the grain boundaries act as barriers for the cross transport of the charge carriers. Many scientists have reported that the origin of the enhanced grain boundary resistivity is due to the presence of double Schottky type space charge barrier layer at the interface. Electronic transport properties can be affected by the polarization field resulting from the ionic displacements of Ti^{4+} and O^{2-} in a TiO_6 octahedron. The *ac* conductivity measurements have been broadly used to investigate the nature of ionic motion in ionically conducting materials since it is assumed that they are responsible for this type of conduction. As known, the electrical behavior of complex ionically conducting materials as a function of frequency shows two regions of behavior named the universally dielectric response and nearly constant loss.

Often, under high voltage fields and high temperatures, the overall resistance of materials is reduced. In order to clearly demonstrate this fundamental phenomenon, we used the *ac* electrical measurements, such as dielectric permittivity, impedance spectroscopy and electric modulus to investigate the detail electrical properties, such as the dielectric relaxation process and the conduction mechanism of the material. Such measurements are very beneficial to distinguish the grain and grain boundary contributions in perovskite-type strontium titanate, which helps in characterizing this material for the desired applications.

The present work undertakes the study of the dielectric properties of $SrTiO_3$ compound using the complex impedance spectroscopy, measured over a wide range of frequency (100 Hz–1 MHz) and with the temperature controlled between 500 and 700 K. In order to investigate the conduction mechanism of this sample, the temperature and frequency dependence of *ac* electrical conductivity properties were studied.

* Corresponding author.
E-mail address: trabelsi.hamdi@rocketmail.com (H. Trabelsi).

https://doi.org/10.1016/j.physe.2018.01.019
Received 16 November 2017; Received in revised form 4 January 2018; Accepted 24 January 2018

2. Experimental details

The STO compound was prepared using the conventional ceramic route. The stoichiometric quantities of $SrCO_3$ and TiO_2 with high-purity (>99.9%) were mixed in an agate mortar and then heated in air at 800 °C for 12 h. The obtained powder was then pressed into pellets (of about 2 mm in thickness and 8 mm in diameter) and sintered at 1100 °C for 2 days and then to 1300 °C for the same duration under oxygen atmosphere with several periods of grinding and repelling. Finally, these pellets were cooled slowly to room temperature in air.

The crystalline phase of the synthesized STO sample was confirmed by XRD analysis using a Siemens D5000 X-ray diffractometer, with monochromator Cu-Kα radiation ($\lambda_{Cu} = 1.5406$ Å), at room temperature. The data was collected in the 2θ range of $20° \leq 2\theta \leq 80°$ with a step scanning of 0.02° and a counting time of 5 s per step.

The morphology of the obtained sample was analyzed by SEM, performed in a Tescan Vega3 system, on the free surface of the material. The sample was sputtered with carbon before microscopic observation. The measurement was conducted in a high vacuum environment, using an electron beam accelerating with a voltage of 25 kV and working distances between 4 and 5 mm.

The characteristic element vibrations in the samples was examined by Raman spectra with a 532 nm laser line through a Horiba, Jobin Yvon HR 800 UV to cross section sample at room temperature. A microscope objective (50 ×) focused the exciting light onto the sample. The spectra were obtained in a back-scattering geometry between 100 and 1400 cm^{-1}.

For this impedance measurement, the opposite sides of the pellet were painted with conductive silver paste. A plane capacitor configuration was obtained, permitting the investigation of the electrical properties of the synthesized material. The measurements were carried out using an Agilent 4294A Precision Impedance Analyzer, in the Cp-Rp configuration over the frequency and temperature range of 100 Hz–1 MHz and 500 K–700 K, respectively. The complex permittivity can be calculated through the measured complex impedance by applying Eqs. (1) and (2) [7]:

$$\varepsilon' = \frac{d}{A}\frac{C_p}{\varepsilon_0} \tag{1}$$

$$\varepsilon'' = \frac{d}{A}\frac{C_p}{\omega R_p \varepsilon_0} \tag{2}$$

where ε' is the real part of the complex permittivity, commonly referred to as dielectric constant, ε'' is the imaginary part of the complex permittivity, also known as the loss factor, C_p and R_p are the parallel capacitance and resistance, respectively, d and A are the sample thickness and electrode area, ω is the angular frequency and ε_0 is the vacuum permittivity (8.8542×10^{-12} F/m).

The complex modulus can be deduced from the complex permittivity values. It is defined as the inverse of the complex permittivity, being the real and imaginary parts given by Eqs. (3) and (4), respectively [8]:

$$M' = \frac{\varepsilon'}{\varepsilon'^2 + \varepsilon''^2} \tag{3}$$

$$M'' = \frac{\varepsilon''}{\varepsilon'^2 + \varepsilon''^2} \tag{4}$$

3. Results and discussion

The XRD diffractogram of the STO sample, obtained at room temperature, is presented in Fig. 1. The result reveals the formation of a single-phase perovskite without any detectable secondary phase within the sensitivity limits of the experiment. The XRD Rietveld refinement was carried out with a *Pm-3m* space group at room temperature by using

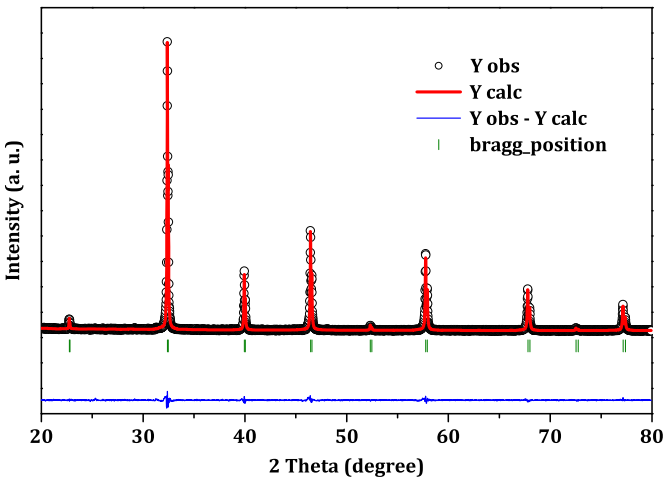

Fig. 1. Rietveld refinement of XRD data of $SrTiO_3$ compound. Solid hollow circle, red line, blue line and green bar mark represent observed, calculated, difference between observed and calculated and Bragg positions respectively. (For interpretation of the references to colour in this figure legend, the reader is referred to the Web version of this article.)

FullProf program [9], and the lattice parameter was 3.905 (8) Å. Based on the Scherrer's equation: $D = 0.89\lambda/\beta \cos\theta$ (where λ is the wavelength of X-ray, θ is the diffraction angle and β is the true half-peak width), the calculated average crystallite size D was 128.4 nm.

Fig. 2a is the SEM image of the free surface of STO sample. It consists of both large and small agglomerated grains characterized by various shapes with some micro-pores, which is in line with our previous results [7]. The measurement and statistical evaluation of the grain size distribution were performed on about 170 particles using the Image-J software. The results are displayed in Fig. 2b as grain number (counts) versus particle size (μm). As it can be seen from this figure, the particles are reasonably monodisperse, and they are distributed according to a Lorentzian law (blue solid line). The estimated average grain size is about 2.135 μm, which is higher than the crystallite size determined previously from the Scherer formula related to X-ray diffraction pattern. The average agglomeration rate, defined as the ratio of the average grain size on that of crystallite, was found to be 16.4.

Fig. 3 depicts the room temperature Raman spectra ranging from 100 to 1400 cm^{-1} with peak deconvolutions for the $SrTiO_3$ sample. The figure discloses two main regions of second order broadband in 220–500 cm^{-1} and at 590–760 cm^{-1}, which are consistent with the results in the literature [2]. The mode observed around 1025 cm^{-1} is also a second-order one. Besides, the peaks near 126 cm^{-1} and 150 cm^{-1} originate from ferroelectric domains induced by oxygen vacancies and *R*-point at the border of Brillouin zone, respectively. However, the peaks observed at 174 cm^{-1}, 540 cm^{-1} and 790 cm^{-1} are assigned to the following first-order modes [10].

The frequency dependence of the real part of dielectric permittivity (ε') and loss tangent ($\tan\delta$) of STO sample as a function of temperatures are shown in Fig. 4. It was noted that the dielectric constant sharply decreased with the increase in frequency (<1 kHz), and the rate of decrease leveled off at high frequencies. However, at relatively low frequency, the dielectric constant strongly depended on frequency, obviously showing a dielectric dispersion. Such a strong dispersion seems to be a common feature in dielectric materials pertaining to ionic conductivity, which is referred to as low-frequency dielectric dispersion [11]. When the frequency increases, the relative effect of ionic conductivity becomes small and, as a result, the frequency dependence of dielectric constant becomes weak. At lower frequencies, the dipolar complexes will be able to keep up with the applied field and reorient with each half cycle. The full effect of the polarization reversal will contribute to the